

# 1 **Elastic recovery of monocrystalline silicon during ultra-fine** 2 **rotational grinding**

3 Ning Huang<sup>1</sup>, Ying Yan<sup>1</sup>, Ping Zhou<sup>1\*</sup>, Renke Kang<sup>1</sup>, Dongming Guo<sup>1</sup> and  
4 Saurav Goel<sup>2,3</sup>

5 <sup>1</sup>Key Laboratory for Precision and Non-traditional Machining Technology of Ministry of Education,  
6 Dalian University of Technology, Dalian 116024, China

7 <sup>2</sup> School of Engineering, London South Bank University, 103 Borough Road, London SE1 0AA, UK

8 <sup>3</sup> School of Aerospace, Transport and Manufacturing, Cranfield University, Bedfordshire, MK43 0AL,  
9 UK

10

## 11 **Abstract**

12 Micromachining of brittle materials like monocrystalline silicon to obtain deterministic  
13 surface topography is a 21<sup>st</sup> Century challenge. As the scale of machining has shrunk  
14 down to sub-micrometre dimensions, the undulations in the machined topography start to  
15 overlap with the extent of elastic recovery (spring back) of the workpiece, posing  
16 challenges in the accurate estimation of the material's elastic recovery effect. The  
17 quantification of elastic recovery is rather complex in the grinding operation due to (i)  
18 randomness in the engagement of various grit sizes with the workpiece as well as (ii) the  
19 high strain rate employed during grinding as opposed to single grit scratch tests employed  
20 in the past at low strain rates. Here in this work, a method employing inclination of  
21 workpiece surface was proposed to quantify elastic recovery of silicon in ultra-fine  
22 rotational grinding. The method uniquely enables experimental extraction of the elastic  
23 recovery and tip radius of the grits actively engaged with the workpiece at the end of the  
24 ultra-fine grinding operation. The proposed experimental method paves the way to enable

---

\* Corresponding author, email: pzhou@dlut.edu.cn

25 a number of experimental and simulation endeavours to develop more accurate material  
26 constitutive models and grinding models targeted towards precision processing of  
27 materials. It can also be shown that using this method if the tip radius distribution of  
28 active grits is measured at different time instances, then this data can be used to assess  
29 the state of the grinding wheel to monitor its wear rate which will be a useful testbed to  
30 create a digital twin in the general framework of digital manufacturing processes.

31 **Keywords:** Brittle materials; rotational grinding; silicon; elastic recovery; grit tip radius

32

### 33 **Abbreviations**

34  $h_e$  : Recovery depth

35  $h_f$  : Residual depth

36  $h$  : Penetration depth

37  $\alpha$  : Coefficient depending on material and geometry

38  $k$  : Coefficient depending on cutting velocity

39  $C$  : Function of  $\alpha$  and  $k$

40  $ERR$ : Elastic recovery ratio ( $h_e/h$ )

41  $TTV$ : Total thickness variation

42

### 43 **1. Introduction**

44 Monocrystalline silicon finds numerous electronic applications due to its excellent  
45 properties such as high hardness, good thermal, chemical stability, and large bandgap  
46 appropriate to be used in the semiconductor industry. Driven by the need for  
47 miniaturization, strenuous efforts are in place to adhere to Moore's Law (which says that  
48 the count of transistors on a silicon chip doubles every two years) which poses a

49 challenging requirement for fabricating ultra-thin silicon wafers (~100  $\mu\text{m}$  thickness)  
50 with deterministic precision [1]. Furthermore, as per the International Technology  
51 Roadmap for Photovoltaics [2], the quality factors affecting yield and costs are total  
52 thickness variation (TTV), surface quality (variations (roughness) and uniformity) and  
53 strength of the wafer (number of defects).

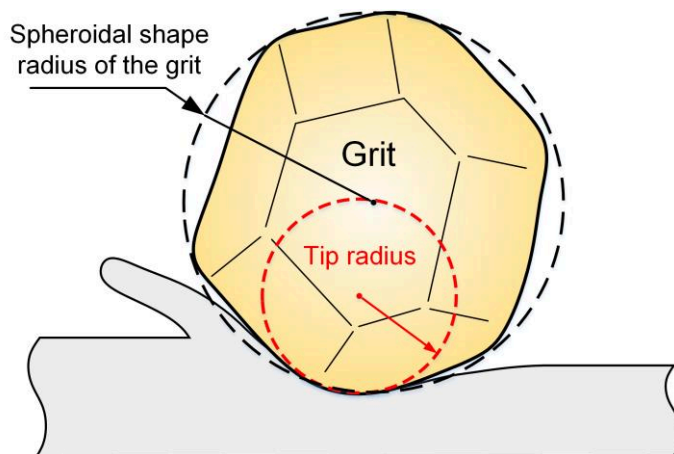
54 Ultra-fine rotational grinding is one of the efficient techniques for fabrication of optical  
55 quality (a root-mean-squares figure accuracy  $< \lambda/10$  with  $\lambda < 1 \mu\text{m}$ ) surfaces in a wide  
56 range of brittle materials including silicon [3]. In the past, the concept of machining brittle  
57 materials in the ductile-mode such that the material removal occurs by virtue of plastic  
58 deformation as opposed to fracture has been well demonstrated in materials ranging from  
59 germanium, silicon and silicon carbide [4-5]. For this reason, various theoretical models  
60 are proposed aimed at optimisation of the rotational grinding process [6-7]. These models  
61 have shown that the quality of the finish depends on grinding parameters, grinding wheel  
62 topography, and stability of the tool-workpiece contact (chatter, vibrations etc.). Besides  
63 these factors, another important factor that leads to deviations from the envisioned  
64 programmable parameters compared to the experimental measurements is inherent to the  
65 material itself, which includes, for example, residual stresses and elastic recovery of the  
66 material that occurs upon release of the cutting load exerted by the moving cutting tool.

67 However, it is worth noting that few reported techniques describe the characterisation  
68 and measurement of the tip radius distribution of actively engaged grits and the material  
69 elastic recovery in ultra-fine rotational grinding up to now. To fill these gaps, a novel  
70 method of grinding on an inclined surface was developed to quantify the extent of elastic  
71 recovery of silicon as well as the tip radius distribution of grinding grits. To our best  
72 knowledge, this is the first paper elucidating the elastic recovery of monocrystalline

73 silicon under the realistic experimental rotational grinding conditions. Likewise, the idea  
74 of being able to monitor the wear of grinding grits with time dependency to align the  
75 grinding process to digital micromanufacturing is being coined for the first time. It is  
76 anticipated that this investigation will have many practical applications in researches on  
77 ultra-fine grinding prediction and optimisation.

## 78 2. Literature review

79 As shown in Fig. 1, most of the research on grinding considers grit tip radius to be  
80 equivalent to an imaginary spheroidal shape radius of the grit and assumes rigid-plastic  
81 material while revealing the effect of the grinding process and wheel parameters on  
82 average attainable depth-of-cut [8-9].



83  
84 Fig. 1. Illustration of the imaginary spheroidal shape tip radius of a grinding grit.

85 Earlier, Zhou et al. [7] proposed a novel model of ultra-fine rotational grinding  
86 incorporating elastic-plastic response of the material and grit tip radius by adding two  
87 coefficients relating to material's elastic recovery and grit tip radius respectively. Their  
88 results show that the simplified assumption of assuming the grit tip radius as equal to the  
89 average grit radius becomes unreasonable in ultra-fine grinding.

90 However, in their work, they did not explicitly discuss the elastic recovery effect of the  
91 material and how it is governed as a function of strain rate. It is known that the strain rate

92 (strain rate = scratching speed/groove width) is positively correlated with scratching  
93 speed for a given groove width. To our best knowledge, few papers expounded on  
94 material elastic recovery in the grinding process. Also, it may be noted that much of the  
95 reported literature [10-14] in material spring back effect had been based on single grit  
96 scratch tests to quantify the elastic recovery of the workpiece whilst scratch experiments  
97 were usually carried out at lower speeds and presented a well-defined work-tool contact  
98 as opposed to the random grit-workpiece contact conditions during the ultra-fine grinding  
99 operation carried out at much higher speeds (strain rates).

100 Other reported papers [15-18] have attempted to measure the topography of the  
101 grinding wheel in terms of the distribution of grits (numbers and size). The reported  
102 measurement methods of grinding wheel topography can be divided into contact mode  
103 and non-contact mode categories [15]. As for contact methods, the topography of the  
104 workpiece is measured by moving the stylus probe across the lay direction with  
105 appropriate consideration of cut-offs and filters [19]. However, contact mode  
106 measurements are limited by the radius of the stylus making it hard to capture fine features  
107 of ultra-fine grits. Another drawback of contact mode measurement is that a stylus or  
108 probe might be caught by crevices when scanning below the outermost surface. Non-  
109 contact wheel measurement methods include 3D optical profilers and Scanning Electron  
110 Microscope (SEM) now known as image-based shape-from-shading (SFS) algorithm [20].  
111 However, non-contact methods can only observe a limited section of the grinding wheel  
112 or would need a destructive preparation of wheel segment, which limits industrial-scale  
113 application.

114 Traditionally, scratch methods (although of a destructive nature) have been useful for  
115 understanding a topography as they produce a longitudinal isolated scratch which can

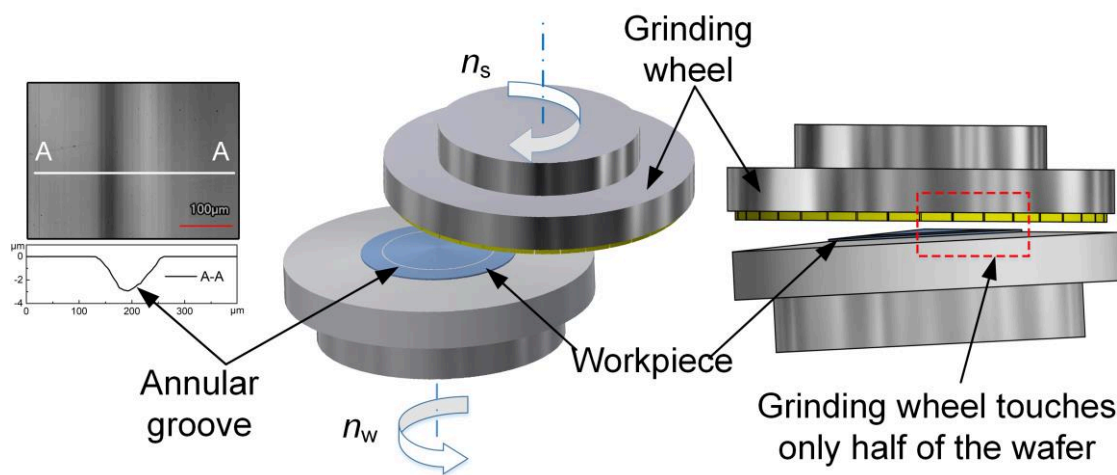
116 easily be analyzed using contact or non-contact mode measurement techniques. In the  
117 case of a rotational grinding operation which has a rotating wheel in its axis, a big  
118 challenge is to isolate the scratch during a single rotation of the wheel that is naturally  
119 overlapped by the subsequent grits. Solutions for avoiding the production of overlapped  
120 surface topography are proposed [21] in the past to obtain an isolated surface topography  
121 either (i) by moving the workpiece at a very fast speed compared to the wheel rotation  
122 speed or (ii) providing an angle of tilt while the wheel and workpiece are moved against  
123 each other. As one can imagine, while implementing the former approach, a compromise  
124 is made in operating at real machining speeds and an inherent speed-dependent influence  
125 would appear in the estimated results. The latter method of tilt angle isolated scratching  
126 exists but to our knowledge, this has not been applied in rotational grinding operations  
127 and this method is yet to be applied and assessed at the nanometric size scale. In the next  
128 section, details of customised experimental assembly are provided where the tilt angle  
129 approach method at the nanoscale was implemented to experimentally obtain the measure  
130 of elastic recovery in the silicon wafer. The new results reported here provide clarity that  
131 the grinding induced elastic recovery ratio (*EER*) is lower than that reported in the past  
132 from the grinding experiments assuming a single grit scratch test..

### 133 **3. Experimental setup and methodology**

134 A schematic diagram of the rotational grinding operation is shown in Fig. 2. As  
135 opposed to other grinding or milling operations, the degree of freedom of the grinding  
136 wheel in this operation are two (one rotation and one axial where pressure is applied) and  
137 this configuration in its original form does not allow the production of isolated scratches.  
138 It is hypothesised that by using a well-defined and structured sloped surface during the  
139 rotational grinding operation, leveraging the aforementioned tilt angle principle will be

140 aided. The novelty in the experiment here is that the rotational angular displacement of  
 141 the wheel was controlled in such a manner that the isolated scratch lengths do not exceed  
 142 the measurement range of an AFM (Atomic Force Microscope) to make all the  
 143 measurements compliant to the AFM. Thus, this configuration helped in testing the tilt  
 144 angle approach at the nanoscale by creating pre-defined scratch lengths and depths in the  
 145 range of several tens of nanometers. The measurements were made along the length of  
 146 the annular groove under the tapping mode until sufficient isolated scratches were  
 147 recorded for subsequent analysis. It should be mentioned here that each residual scratch  
 148 was assumed to represent a single grit in this study because tiny diamond grits are hardly  
 149 broken to form multiple cutting edges which are a valid assumption taken into  
 150 consideration in previous studies [22]. Therefore, the statistics of the numbers and heights  
 151 of residual grooves represent those formed by the active grits.

152



153

154 Fig. 2. Illustration of the scratch method based on rotational grinding. An annular groove was  
 155 processed by polishing the (100) surface of Silicon before grinding with a highly protruded grit. The  
 156 topography of isolated grinding scratches on the grooved surface provided detailed information about  
 157 wheel topography and material response.

158

159 The grinding wheel used was a diamond cup wheel. Wafer grinding was carried out  
160 after wheel dressing to ensure a stable working state of the grinding wheel and to avoid  
161 the impact of grinding wheel dressing and wear on the experimental results. An annular  
162 groove of diameter 75 mm was created by the polishing method on the surface of the  
163 commercially available silicon (100) wafer of diameter 200 mm. The cross-sectional  
164 profile (Section A-A) of this groove is shown in Fig. 2. An ultrafine grinding machine  
165 (VG401 MK II, Okamoto, Japan) was employed to grind the sample surface with grinding  
166 wheels of two mesh sizes, SD600 and SD3000 to ensure the robustness in the reported  
167 results. Grinding wheels of these sizes are commonly used in the back-grinding of the  
168 wafer thinning process. During the grinding process, both the wheel and the wafer rotated  
169 around their axes, and the wheel was gently directed into the workpiece by moving it  
170 along the axial direction at a prescribed velocity. The wafer elastically complies to the  
171 curved shape presented by the chuck thus ensuring the grinding wheel touches only half  
172 of the wafer shown in Fig. 2. More details about the grinding wheel and the process  
173 parameters used are provided in Table 1. The selection of these parameters was primarily  
174 governed by typical industrial practice to obtain elastic recovery of silicon under actual  
175 grinding process. It is known that different parameters lead to a variation in the cutting  
176 depth of the grits. In this study, the design of the sloped surface (polished groove) enables  
177 observation of isolated scratches with gradually increased depth of cut. Therefore, the  
178 variation of grit depth of cut due to varied parameters will not affect the practical value  
179 of this experimental results.

180 An Atomic force microscope (XE-200, Park Systems, Korea) was used to measure the  
181 isolated scratches under tapping mode. The nominal position detector noise of the AFM  
182 used in this study was less than 0.1 nm and the measurement uncertainty was about 0.3



183 nm, much smaller than the characteristic size of the scratch. The measured length  $l$  of  
 184 samples ground by wheel SD600 and SD3000 was 0.924 mm and 0.177 mm, respectively.

185 Table 1 Details of grinding wheel and process parameters

Mesh no.	Segment width, $w$ (mm)	Wheel diameter (mm)	Rotational speed		Feed, $f$ ( $\mu\text{m}/\text{rpm}$ )
			Wheel, $n_w$ (rpm)	Wafer, $n_s$ (rpm)	
SD600	3	350	2399	60	30/60=0.5
SD3000	3	350	2399	100	10/100=0.1

186

187

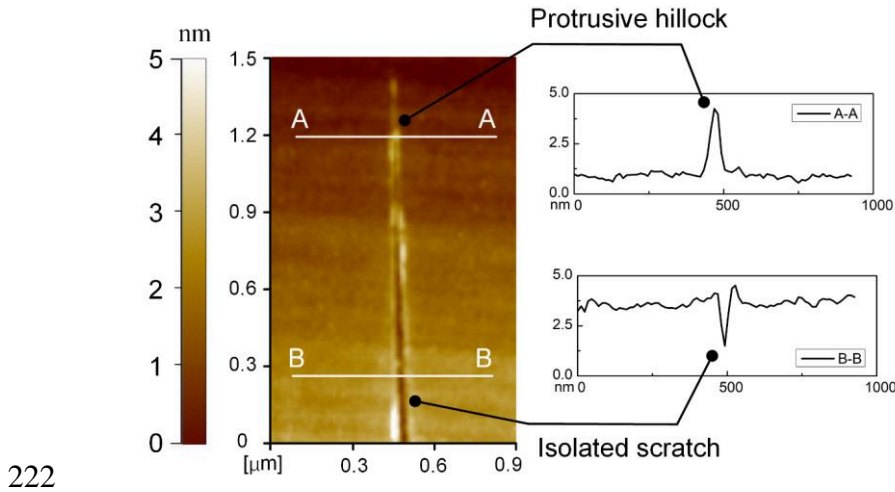
## 188 4. Results and discussions

### 189 4.1 Material's elastic recovery

190 Material's elastic recovery in the micromachining process refers to the tendency of the  
 191 finished machined surface to recover elastically (spring back effect) after the tool has  
 192 moved away. The material's elastic recovery ratio can be derived from isolated scratch  
 193 topography. The interaction between an individual active grit tip and the workpiece is  
 194 depicted in Fig. 3. Point A indicates where the active grit begins to interact with the  
 195 workpiece. Constructed dashed line AB parallel to the ground surface through point A  
 196 shows the programmed depth of cut revealing an ideal cutting tool path. Point C to Point  
 197 D highlighted by a green area represents the extent of elastic recovery. The distance from  
 198 point E to line AB represents the penetration depth  $h$  and point D to line AB represents  
 199 the elastic recovery depth  $h_e$ , respectively. So in essence,  $h$  was the programmed depth of  
 200 cut and experimentally one would obtain  $h-h_e$  as the measured depth of cut.



220 similar observation reported in Qian's work [24-25]. A sample structure measured by an  
 221 AFM to highlight this hillock-like protrusive structure is shown in Fig.4.



222  
 223 Fig. 4. A hillock-like protrusive nanostructure at the beginning of an isolated scratch measured by an  
 224 AFM.

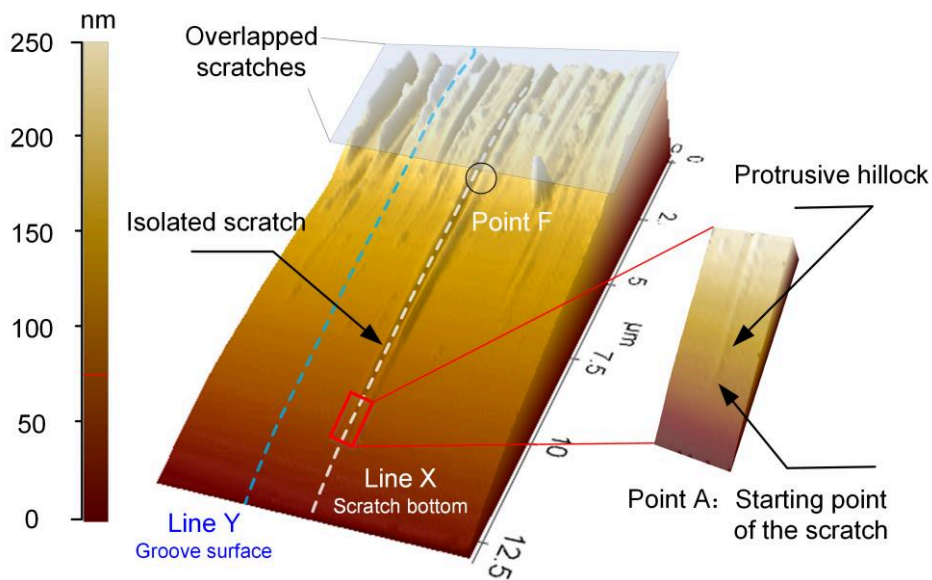
225 The previous study has demonstrated that these hillocks are induced by a combination  
 226 of oxidation reaction and mechanical interaction and the critical contact stress  $\sigma$  for their  
 227 formation was reported to be 11.1 GPa [24] – This is although a possible future area of  
 228 research as to what conditions lead to the formation of these structures. The penetration  
 229 depth of the grit at this point can be estimated by Hertzian theory [26]:

230

$$231 \quad h_{\text{cri}} = \frac{\pi^2 \sigma^2 R_{\text{tip}}}{4E^2} \approx 0.019R_{\text{tip}} \quad (1)$$

232 where the reduced elastic modulus  $E$  for (100) silicon is about 126 GPa [27]. The tip  
 233 radius  $R_{\text{tip}}$  was about one-tenth of the grit size, so the penetration depth of grits in the  
 234 elastic-regime is only a few nanometers, which is much smaller than the maximum  
 235 penetration depth-of-cut. Therefore, the position of the hillock is assumed to be the  
 236 starting position of the interaction of the grits with the workpiece, i.e. the starting point A  
 237 in Fig. 3.

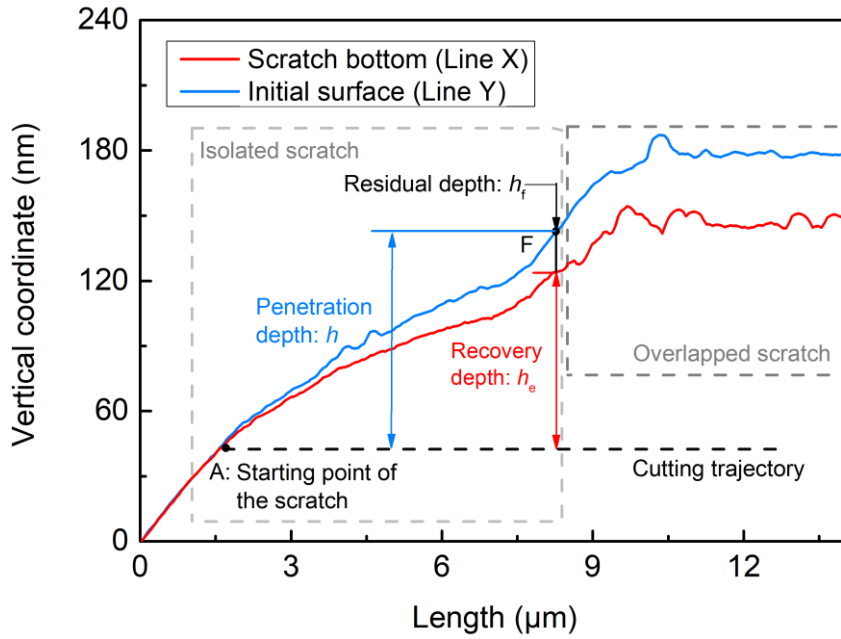
238 One example of the results obtained for a single isolated scratch is shown in Fig. 5.  
 239 Line X in Fig. 5(a) represents the height of an isolated scratch bottom, while line Y  
 240 represents the height of the groove surface giving a slope of about  $0.72^\circ$ . Line Y (shown  
 241 in 2D representation in Fig. 5(b)) represents the datum surface of the isolated scratch  
 242 considering the continuity of the groove surface. Both lines are shown and plotted in  
 243 Fig. 5(b). Fig. 5(b) shown in 2D was plotted by taking the bottom coordinate of the scratch  
 244 profile in 3D thus considering the entire width and length of the isolated scratch.  
 245 Therefore, the penetration depth  $h$  and the elastic recovery depth  $h_e$  is the difference  
 246 between the datum surface (blue line) and scratched surface (red line) with respect to  
 247 Point A shown in Fig. 5(b). It may be noted that the value of  $h_e$  varies at various points  
 248 along the length of the scratch starting from Point A to Point F which represents an  
 249 isolated scratch length. Beyond Point F, the scratch profile was overlapped by the other  
 250 grits.



251

252

(a)



253

254

(b)

255 Fig. 5. An example of the residual depth  $h_r$  and penetration depth  $h$  obtained for a single isolated  
 256 scratch. Point A in (a) shows a hillock-like protrusive nanostructure at the beginning of the scratch.  
 257 Line X represents the height of an isolated scratch bottom, while line Y represents the height of the  
 258 groove surface.

259

260 For statistical analysis, over 100 isolated scratches were analyzed for both types of  
 261 wheels. The sampling area where these scratches were collected was randomly selected  
 262 on the surface of the polished groove, then isolated scratches on the surface of the  
 263 sampling area were analyzed one by one to ensure the results robustly and reproducibly.  
 264 To understand the influence of grit size, speed of scratch and influence of material  
 265 properties on the depth of recovery ( $h_e$ ), indentation theory proposed by Oliver and  
 266 Pharr [27] was used to develop a semi-empirical analytical model. The recovery depth  
 267 ( $h_e$ ) and penetration depth ( $h$ ) geometrically apply to the following equation:

268

$$h_r = h - h_e \quad (2)$$

269 where  $h_f$  is residual depth of an isolated scratch. For spherical tool tips, the resultant  
 270 normal force  $P$  can be calculated from:

$$271 \quad P = \alpha h_e^{\frac{3}{2}} = \alpha (h - h_f)^{\frac{3}{2}} \quad (3)$$

272 where  $\alpha$  is a constant related to workpiece material and the grit size. Based on the results  
 273 on high-speed nano-cutting tests [28], the resultant normal force  $P$  can also be written as  
 274 a linear function of residual depth  $h_f$ :

$$275 \quad P = kh_f \quad (4)$$

276 where coefficient  $k$  is a constant depending on cutting velocity. Comparing Eq. (3) and  
 277 Eq. (4) gives:

$$278 \quad kh_f = \alpha (h - h_f)^{\frac{3}{2}} \quad (5)$$

279 Adjustment of variables from Eq. (2) and (5) gives:

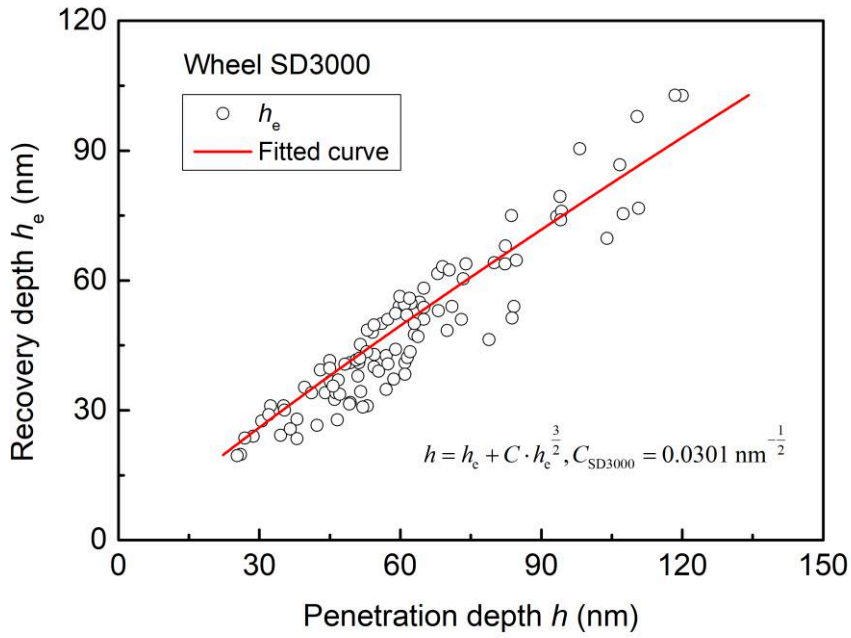
$$280 \quad h = h_e + Ch_e^{\frac{3}{2}} \quad (6)$$

$$281 \quad C = \frac{\alpha}{k} \quad (7)$$

282 where  $C$  is a strong function of  $\alpha$  (*grit size dependence*) and  $k$  (*scratch speed dependence*).  
 283 In this work, the grit was approximated as being spherical, and the cutting speed was kept  
 284 the same during the grinding process. Therefore, coefficient  $C$  for wheel SD3000 (typical  
 285 average grit size  $\sim 5 \mu\text{m}$ ) and SD600 (typical average grit size  $\sim 25.3 \mu\text{m}$ ) at the same  
 286 operational cutting speed ( $k$  being the same) was obtained as  $0.0301 \text{ nm}^{-1/2}$  and  
 287  $0.1004 \text{ nm}^{-1/2}$  respectively signifying that the increase in grit size leads to an increase in  
 288 the value of  $C$ , as shown in Fig. 6(a) and Fig. 6(b). The fitted results were further used to  
 289 evaluate the material elastic recovery ratio (*ERR*) during the grinding process:

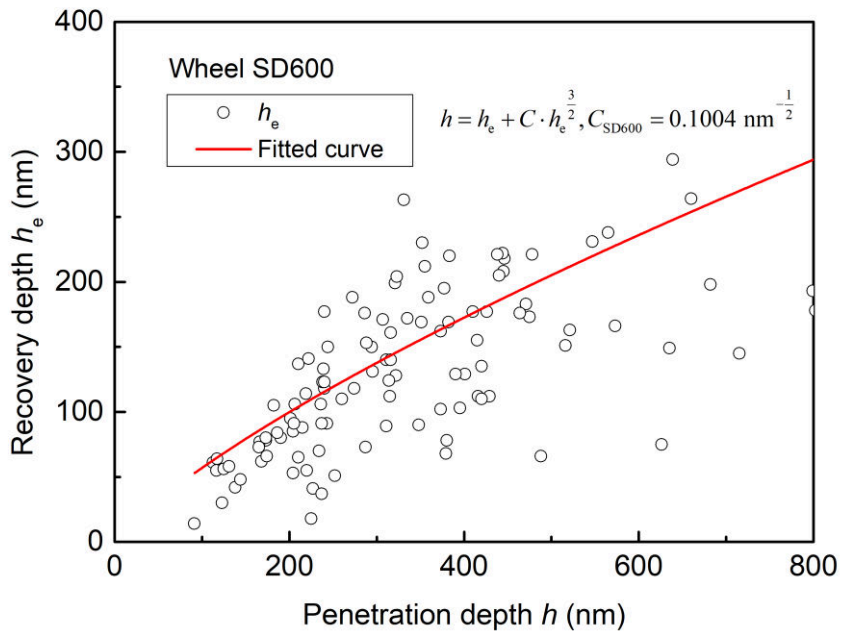
290

$$ERR = \frac{\text{Recovery depth } (h_e)}{\text{Penetration depth } (h)} \quad (8)$$



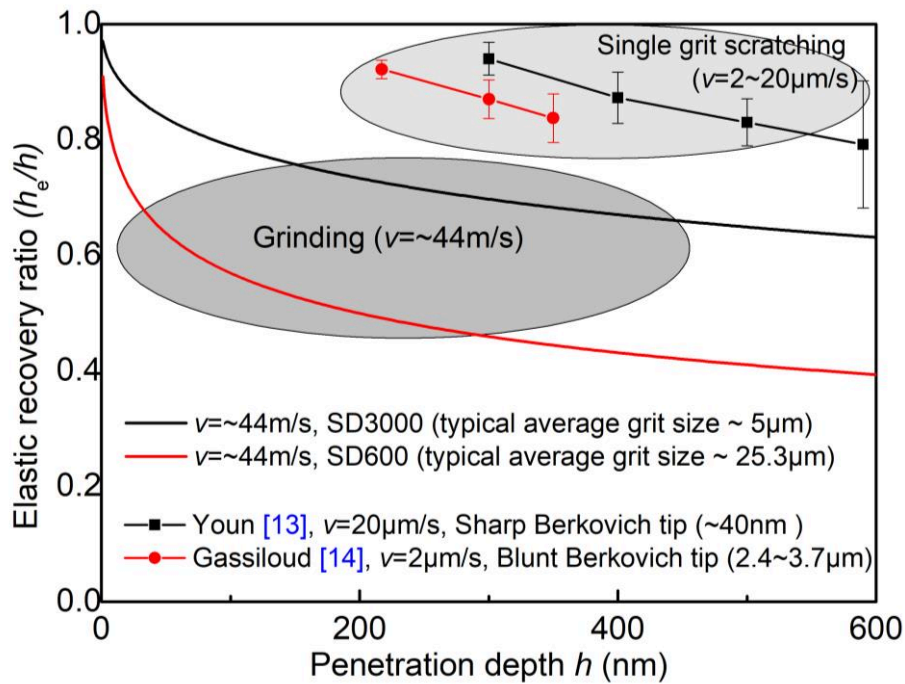
291  
292

(a)



293  
294

(b)



295  
296

(c)

297 Fig. 6. Elastic recovery depth  $h_e$  as a function of penetration depth  $h$  for wheel size of (a) SD3000 and  
 298 (b) SD600. Both plots were fitted by the semi-empirical model (Eq. (6)) and (c) Elastic recovery ratio  
 299 ( $h_e/h$ ) was plotted against penetration depth for both wheels.

300

301 The calculated *ERR* is plotted in Fig. 6(c) against the penetration depth. Due to the  
 302 differences in the grit sizes, the *ERR* shown by the wheel SD3000 was larger than that of  
 303 SD600 for the same penetration depth and the same scratch speed. At this point, it's worth  
 304 comparing these results obtained by the grinding conditions with results obtained by the  
 305 single grit scratch conditions, which was the motivation in pursuing this research study.

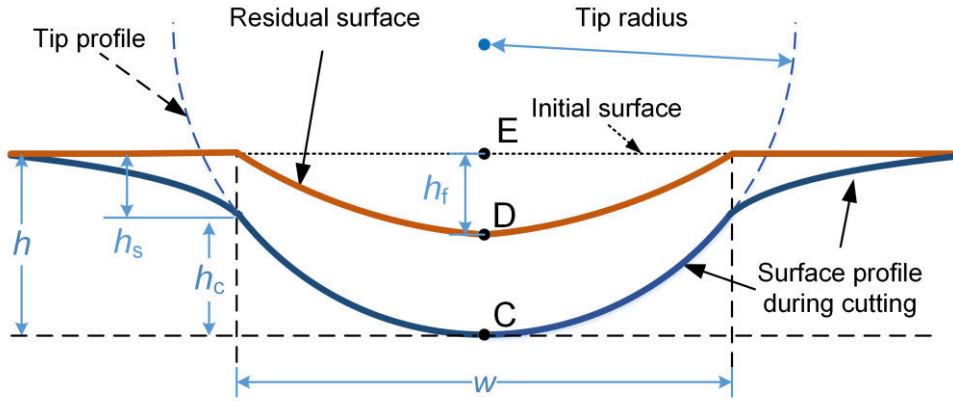
306 The material elastic recovery of the (100) silicon during two reported single grit scratches  
 307 carried out by Gassilloud [13] (scratch speed  $v = 2 \mu\text{m/s}$ , blunt Berkovich tip with  
 308 estimated tip radius of  $2.4\sim 3.7 \mu\text{m}$ ) and Youn [14] (scratch speed  $v = 20 \mu\text{m/s}$ , sharp  
 309 Berkovich tip with an estimated tip radius of  $40 \text{ nm}$ ) are compared in the plot Fig.6(c)  
 310 with error bars indicating standard deviation. The previously reported scratch tests were



311 performed at low scratch velocities than an experimental grinding speed used in this study.  
312 These results indicate that (i) smaller tip radius and lower cutting speed (low strain rate)  
313 results in higher material elastic recovery for given penetration depth, and (ii) elastic  
314 recovery of silicon would not change significantly unless the cutting speed or strain rate  
315 changes more than one magnitude. In rotational grinding of silicon, the wheel speed is  
316 the decisive factor that determines the speed of grits relative to the workpiece compared  
317 to the workpiece speed. The wheel speed typically varies between 2000 rpm and  
318 3500 rpm according to industrial practice. Therefore, the results of this study performed  
319 at a wheel speed of 2400 rpm can serve as a reference for evaluating material recovery in  
320 silicon grinding. The data of grinding group and single grit scratch group in Fig.6(c) also  
321 shows that when cutting speed of grits is small, the size of the grit cutting tip is a crucial  
322 factor influencing the amount of material elastic recovery for given penetration depth.  
323 This helps explain why the fitting of SD 600 wheel in Fig. 6(b) is much worse than the  
324 fitting of SD3000 in Fig.6(a) because the variation of grit tip size of SD600 is much larger  
325 than that with wheel SD3000, which was discussed in the following section 4.2.  
326 Following the aforementioned results, it is reasonable to infer that elastic recovery of the  
327 material makes a significant influence on the form deviations (in the nm scales) and it is,  
328 therefore, imperative to consider this aspect in developing the grinding models.

#### 329 4.2 Grit tip radius

330 The previous sections were focused on obtaining the residual depth  $h_f$  and penetration  
331 depth  $h$  by measuring an isolated scratch topography. This section describes the procedure  
332 to obtain actively engaged grit tip radius. Fig. 7 shows a typical illustration of the  
333 spherically shaped single grit engagement with the workpiece at a particular instance  
334 adopted from the nanoindentation theory proposed by Oliver and Pharr [27].



335

336 Fig. 7. A schematic illustration of a transverse cross-sectional view of residual isolated scratch. Points  
 337 C, D, and E correspond to those in Fig. 3. Here  $h_c$  refers to contact depth, and  $h_s = h - h_c$  refers to vertical  
 338 displacement at the contact perimeter. It is generally assumed that the contact width of the tool tip is  
 339 equal to the residual width  $w$  of the groove [27, 29-30].

340

341 The contact depth  $h_c$  showed in Fig. 7 can be obtained by knowing the residual depth  
 342  $h_f$  and penetration depth  $h$  [27]:

$$343 \quad h_s = \frac{\pi - 2}{\pi} (h - h_f) \quad (9)$$

$$344 \quad h_c = h - h_s \quad (10)$$

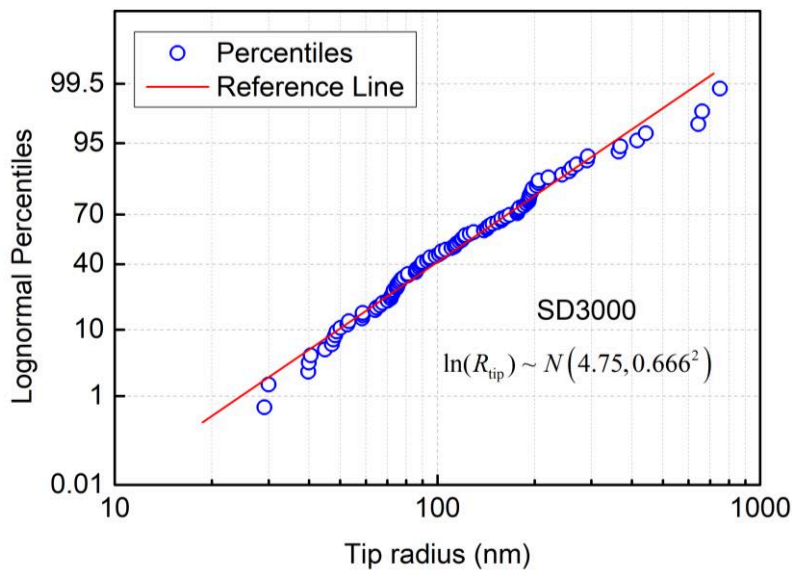
345 where  $h_s$  is the vertical displacement at the contact perimeter. The contact depth  $h_c$  can  
 346 accommodate the residual depth  $h_f$  and penetration depth  $h$  by substituting Eq. (9) into  
 347 Eq. (10):

$$348 \quad h_c = \frac{2}{\pi} h + \frac{\pi - 2}{\pi} h_f \quad (11)$$

349 It is generally assumed that the residual width  $w$  of the groove is equal to the contact  
 350 width of the tool tip [27, 29-30]. Thus, the tip radius can be geometrically calculated as:

$$351 \quad R_{\text{tip}} = \frac{h_c}{2} + \frac{w^2}{8h_c} \quad (12)$$

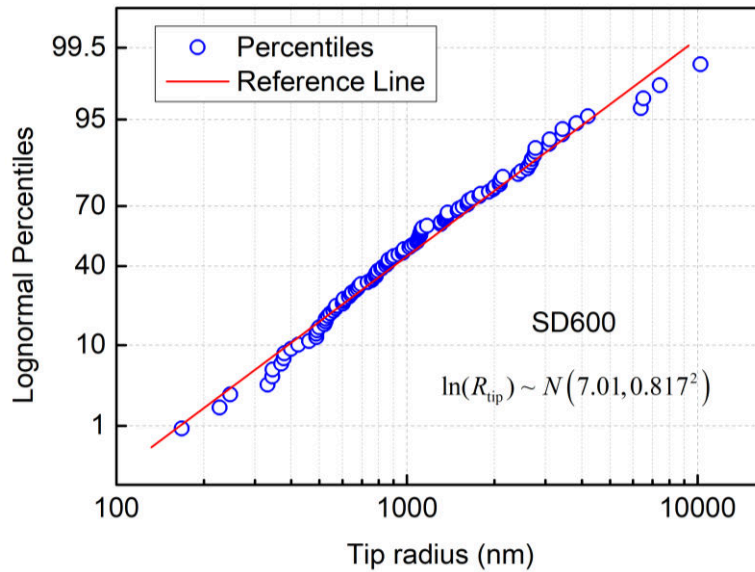
352 With Eq. (12), a statistical topography measurement of residual scratches can be used  
 353 to evaluate the distribution of the tip radius. The calculation error of grit tip radius caused  
 354 by the measurement error of penetration depth was estimated to be less than 5% according  
 355 to Eq. (1) and Eq. (12). With this statistical data, the lognormal probability plot of the grit  
 356 tip radius (scatter) is plotted in Fig. 8 against a theoretical lognormal distribution set (red  
 357 line). The scatter points are close to the theoretical line which indicates that the grit tip  
 358 radius can be well described by the lognormal distribution. Further calculations show that  
 359 the natural logarithm of grit tip radius of wheel SD3000 and SD600 follows  $N(4.75,$   
 360  $0.666^2)$  and  $N(7.01, 0.817^2)$ , respectively. The grit tip radius proves to be much smaller  
 361 than the average grit radius. Hence, lognormal distribution of grit tip radius instead of  
 362 average grit radius can be used when building models for the ultra-fine grinding process.



363

364

(a)



365

366

(b)

367 Fig. 8. Lognormal probability plot of the grit tip radius of wheel SD3000 (a) and SD600 (b). The  
 368 experimental data set (scatter) is plotted against a theoretical lognormal distribution set (red line). The  
 369 scatter points are close to the theoretical line which indicates that the grit tip radius can be well  
 370 described by the lognormal distribution.

#### 371 4. Conclusions

372 This paper provides a fresh experimental methodology to obtain the in-process  
 373 measurement of material elastic recovery during the grinding process, hitherto not  
 374 reported in the extant literature covering rotational grinding. Beside numerous findings  
 375 that are reported within the paper, an active contribution this paper makes is to provide  
 376 valuable experimental data of the extent of elastic recovery of monocrystalline silicon  
 377 made during the experimental grinding conditions as opposed to previously reported  
 378 single grit scratch tests which were only indicative but were not thorough enough to  
 379 support modelling activities in this area. Based on the experimental results, a semi-  
 380 empirical analytical model was developed, and the combined observations made from the  
 381 analytical model and the experiments can be concluded as follows:

- 382 1. Isolated scratch trajectories are more relevant and meaningful than the overlapped  
383 scratch trajectories to infer and extract relevant data from the surface topography  
384 to study the problems in ultra-fine rotational grinding of monocrystalline silicon.
- 385 2. Elastic recovery depth (defined as  $h_e$ ) was found to increase monotonically with the  
386 increase in penetration depth whilst the elastic recovery ratio (defined as  $h_e/h$ )  
387 decreases monotonically with increased penetration depth. These combined  
388 observations and comparison with single grit scratching tests pointed to the fact  
389 that the larger grit size and a coarser grinding wheel operated at a higher speed  
390 leads to a lesser extent of elastic recovery of silicon.
- 391 3. Much like the published literature on the topic of silicon nano-scratching, even  
392 during the precision grinding operation, hillock-like protrusive nanostructures were  
393 observed to form at the beginning of the scratch process and are an interesting area  
394 of exploration for future research.
- 395 4. The grit tip radius was found to follow a lognormal distribution and it turns out that  
396 the active grit tip radius is much smaller than the average grit radius. Hence,  
397 lognormal distribution of grit tip radius instead of average grit radius is a more  
398 appropriate measure while building suitable models of the ultra-fine rotational  
399 grinding process.

#### 400 **Acknowledgments**

401 All authors appreciate the financial support from the National Natural Science  
402 Foundation of China (51875078, 51991373, 51975094), and the Science Fund for  
403 Creative Research Groups of NSFC of China (51621064). The cross-exchange became  
404 possible due to the financial support provided by the UKRI to SG via Grants No.:  
405 (EP/K503241/1, EP/L016567/1, EP/S013652/1, EP/T001100/1, EP/S036180/1 and

406 EP/T024607/1). Part of this work used Isambard Bristol, UK supercomputing service  
407 accessed by the Resource Allocation Panel (RAP) grant. SG is particularly grateful to  
408 the fantastic financial support provided by H2020 (Cost Actions (CA15102, CA18125,  
409 CA18224 and CA16235)), EURAMET EMPIR A185 (2018), Royal Academy of  
410 Engineering (Grant No. IAPP18-19\295- Indo-UK partnership and Grant No. TSP1332  
411 - South Africa- UK partnership) and Newton Fellowship award from the Royal  
412 Society (NIFAR1\191571).

413

414 **References**

- 415 [1] Goel S, Kovalchenko A, Stukowski A, Cross G. Influence of microstructure on the  
416 cutting behaviour of silicon. *Acta Mater.*, 2016, 105, 464-478.
- 417 [2] International Technology Roadmap for Semiconductors. <http://www.itrs.net> (2015)
- 418 [3] Brinksmeier E, Mutlugünes Y, Klocke F, Aurich J C, Shore P, Ohmori H. Ultra-  
419 precision grinding. *CIRP Ann. Manuf. Technol.*, 2010, 59(2), 652-671.
- 420 [4] Goel S, Luo X, Comley P, Reuben R L, Cox A. Brittle–ductile transition during  
421 diamond turning of single crystal silicon carbide. *Int. J. Mach. Tools Manuf.*, 2013,  
422 65: 15-21.
- 423 [5] Goel S, Luo X, Agrawal A, Reuben R L. Diamond machining of silicon: a review of  
424 advances in molecular dynamics simulation. *Int. J. Mach. Tools Manuf.*, 2015, 88:  
425 131-164.
- 426 [6] Young H T, Liao H T, Huang H Y. Novel method to investigate the critical depth of  
427 cut of ground silicon wafer. *J. Mater. Process. Technol.*, 2007, 182(1-3): 157-162.
- 428 [7] Lin B, Zhou P, Wang Z G, Yan Y, Kang R K, Guo D M. Analytical Elastic–Plastic  
429 Cutting Model for Predicting Grain Depth-of-Cut in Ultrafine Grinding of Silicon  
430 Wafer. *J. Manuf. Sci. Eng.-Trans. ASME*, 2018, 140(12): 121001.

- 431 [8] Zhou L, Tian Y B, Huang H, Sato H, Shimizu J. A study on the diamond grinding of  
432 ultra-thin silicon wafers. *Proc. Inst. Mech. Eng. Part B-J. Eng. Manuf.*, 2012, 226(1):  
433 66-75.
- 434 [9] Pei Z J, Strasbaugh A. Fine grinding of silicon wafers. *Int. J. Mach. Tools Manuf.*,  
435 2001, 41(5): 659-672.
- 436 [10] Ge M, Zhu H, Huang C, Liu A, Bi W. Investigation on critical crack-free cutting  
437 depth for single crystal silicon slicing with fixed abrasive wire saw based on the  
438 scratching machining experiments. *Mat. Sci. Semicon. Proc.*, 2018, 74: 261-266.
- 439 [11] Aurich J C, Steffes M. Single grain scratch tests to determine elastic and plastic  
440 material behavior in grinding. *Advanced Materials Research. Trans Tech*  
441 *Publications Ltd*, 2011, 325: 48-53.
- 442 [12] Öpöz T T, Chen X. Experimental investigation of material removal mechanism in  
443 single grit grinding. *Int. J. Mach. Tools Manuf.*, 2012, 63: 32-40.
- 444 [13] Gassilloud R, Ballif C, Gasser P, Buerki G, Michler J. Deformation mechanisms of  
445 silicon during nanoscratching. *Phys. Status Solidi A-Appl. Res.*, 2005, 202(15):  
446 2858-2869.
- 447 [14] Youn S W, Kang C G. A study of nanoscratch experiments of the silicon and  
448 borosilicate in air. *Mat. Sci. Eng. A-Struct.*, 2004, 384(1-2): 275-283.
- 449 [15] McDonald A, Bauer R, Warkentin A. Design and validation of a grinding wheel  
450 optical scanner system to repeatedly measure and characterize wheel surface  
451 topography. *Measurement*, 2016, 93: 541-551.
- 452 [16] Ye R, Jiang X, Blunt L, Cui C, Yu Q. The application of 3D-motif analysis to  
453 characterize diamond grinding wheel topography. *Measurement*, 2016, 77: 73-79.

- 454 [17]Tahvilian A M, Liu Z, Champlaud H, Hazel B, Lagacé M. Characterization of  
455 grinding wheel grain topography under different robotic grinding conditions using  
456 confocal microscope. *Int. J. Adv. Manuf. Tech.*, 2015, 80(5-8): 1159-1171.
- 457 [18]Darafon A, Warkentin A, Bauer R. Characterization of grinding wheel topography  
458 using a white chromatic sensor. *Int. J. Mach. Tools Manuf.*, 2013, 70: 22-31.
- 459 [19]Leach R K. Measurement Good Practice Guide No. 37, The measurement of surface  
460 texture using stylus instruments. National Physical Laboratory, Ed, 2001.
- 461 [20]Wang J, Su R, Leach R, Lu W, Zhou L, Jiang X. Resolution enhancement for  
462 topography measurement of high-dynamic-range surfaces via image fusion. *Opt.*  
463 *Express*, 2018, 26(26): 34805-34819.
- 464 [21]Malkin Stephen, Changsheng Guo. Grinding technology: theory and application of  
465 machining with abrasives. Industrial Press Inc., 2008.
- 466 [22]Zhou L, Ebina Y, Wu K, Shimizu J, Onuki T, Ojima H. Theoretical analysis on  
467 effects of grain size variation. *Precis. Eng.*, 2017, 50: 27-31.
- 468 [23]Zhang Z, Yan J, Kuriyagawa T. Study on tool wear characteristics in diamond turning  
469 of reaction-bonded silicon carbide. *Int. J. Adv. Manuf. Tech.*, 2011, 57(1-4): 117-  
470 125.
- 471 [24]Yu B, Dong H, Qian L, Chen Y, Yu J, Zhou Z. Friction-induced nanofabrication on  
472 monocrystalline silicon. *Nanotechnology*, 2009, 20(46): 465303.
- 473 [25]Yu B, Li X, Dong H, Chen Y, Qian L, Zhou Z. Towards a deeper understanding of  
474 the formation of friction-induced hillocks on monocrystalline silicon. *J. Phys. D*  
475 *Appl. Phys.*, 2012, 45(14): 145301.
- 476 [26]Johnson K L. Contact mechanics. Cambridge university press, 1987.



- 477 [27] Oliver W C, Pharr G M. An improved technique for determining hardness and elastic  
478 modulus using load and displacement sensing indentation experiments. *J. Mater.*  
479 *Res.*, 1992, 7(6): 1564-1583.
- 480 [28] Huang N, Yan Y, Zhou P, Kang R, Guo D. Elastic-plastic deformation of single-  
481 crystal silicon in nano-cutting by a single tip tool. *Jpn. J. Appl. Phys*, 2019.
- 482 [29] Jing X, Maiti S, Subhash G. A new analytical model for estimation of scratch -  
483 induced damage in brittle solids. *J. Am. Ceram. Soc.*, 2007, 90(3): 885-892.
- 484 [30] Kaupp G. Atomic force microscopy, scanning nearfield optical microscopy and  
485 nanoscratching: application to rough and natural surfaces. Springer Science &  
486 Business Media, 2006.
- 487